IEEE Access
Multidisciplinary | Rapid Review | Open Access Journal

Received 10 January 2024, accepted 26 January 2024, date of publication 1 February 2024, date of current version 12 February 2024.

Digital Object Identifier 10.1109/ACCESS.2024.3361280

RESEARCH ARTICLE

Discrete Centralized AGC Using LQR-Based Cost Functional Minimization for Multi-Area Interconnected Power Systems

MOHAMMED ESMAIL AND SENTHIL KRISHNAMURTHY, (Member, IEEE)
Center for Substation Automation and Energy Management Systems, Department of Electrical, Electronic and Computer Engineering, Cape Peninsula University of Technology, Cape Town 7535, South Africa

Corresponding author: Mohammed Esmail (esmailmy73@gmail.com)

This work was supported in part by the NRF Thuthuka under Grant 138177, and in part by the Eskom Tertiary Education Support Programme (TESP).

ABSTRACT This paper proposes the design of Discrete Centralized Optimal Quadratic Automatic Generation Control (COQAGC) based on the functional minimization method (FMM) and optimal control theory for interconnected power systems. The cost function and FMM design requirements are defined in terms of area control errors, integral area control errors, and control signals. FMM is an optimal method, an easy and systematic approach for constructing and selecting state and control weighting matrices. The performance of COQAGC on discrete two-area interconnected power systems with identical _non-reheat thermal turbines has been studied using 1% and 5% step load perturbations (*SLPs*) and sensitivity analysis. The study has been extended to investigate the performance of COQAGC on discrete multi-area multi-source interconnected power systems with wind turbines. The simulation results revealed that developed COQAGC-based FMM improves the power system dynamics in terms of the steady-state performance and robustness against *SLPs* and parameter variations in comparison with controllers from the literature. The developed method can be extended and implemented on large complex multi-area power systems.

INDEX TERMS Automatic generation control, functional minimization method, interconnected power systems, optimal LQR control, weighting matrices.

NOMENCLATURE AND ABBREVIATIONS

ΔP_{tie12}: Tie-line power deviation between control areas 1 and 2.
Δf_i: Deviation in frequency for the ith area (Hz) (i = 1, 2).
ΔP_{Ti}: The deviation in the power output of the turbine for the ith area (pu.MW).
ΔP_{Gi}: The deviation in the governor valve position for the ith area (pu.MW).
ΔP_{Di}: The load input deviation for the ith area (pu.MW).
$IAEC_i$: The integral deviation of area control error for ith area.
T_{psi}: Power system time constant for the ith area (s).
T_{ti}: Turbine time constant for the ith area (s).
T_{Gi}: Governor time constant for the ith area (s).
T_{ij}: Tie-line synchronizing coefficient between the ith area and jth area (pu.MW).
k_{psi}: The power system's gain for the ith area.
ACE_i: Area control error for the ith area.
R_i: Speed regulation due to the governor action for the ith area (Hz.pu. MW^{-1}).
B_i: Frequency biasing factor for the ith area.
x: = The states of the overall interconnected power system.
L : The quadratic optimal control constant vector for the control area.
u_i: The control law signal for the ith area.
N: Number of interconnected power systems.

The associate editor coordinating the review of this manuscript and approving it for publication was Engang Tian.

COQAGC:	Discrete centralized optimal quadratic Automatic generation control.
FMM:	Functional minimization method.
SLPs:	Step load perturbations.
AGC:	Automatic Generation Control.
PV:	Photovoltaic.
ANFIS:	Adaptive Neuro-Fuzzy Interference System.
FOBELBIC:	Fractional order brain emotional learning based intelligent controller.
FOPID:	Hybrid type-2 fuzzy logic controllers with fractional order proportional integral derivative.
ADRC:	Active Disturbance Rejection Control.
LQR:	Linear Quadratic Regulator.
Q:	State cost weighing matrix.
R:	Control cost weighting matrix.
PSO:	Particle swarm optimization.
ODEs:	Ordinary differential equations.
I:	An identity matrix a.
T:	Sampling periods.
GCOAQGC:	Continuous Global centralized optimal quadratic automatic generation.
TLBO-PIDD:	Teaching learning-based optimization proportional integral double derivative.
FGSC:	Fuzzy Gain Scheduling Controller.
POS:	Peak Overshoot.
STs:	Settling Times.
DRRT:	Disturbance Rejection Response Time.
T12:	Tie-line synchronization coefficient between two area control interconnected power systems.
α:	The vector of participation factors.
U_{th1}, U_{hy}, U_w and U_{th2}:	Control signals applied to non-reheat thermal 1, hydro, wind turbine, and non-reheat thermal 2 plants respectively.
GRC:	Generation Rate Constraint.
OFSFC:	Optimal Full-State Feedback Control.
LFC:	Load Frequency control.
LFC-MGOA:	LFC-based Modified Grasshopper Optimization Algorithm.
PUS:	Peak Undershoot.
CSLPs:	Concurrent Step Load Perturbations.
$e_{ss}(\infty)$:	Steady state error.
ITAE:	Integral Multiplied Time Absolute Error.
ΔP_{hy} :	Deviation in hydro unit output (pu).
ΔX_h :	Deviation in an intermediate state of the mechanical hydraulic governor.
ΔP_{rh} :	Deviation in intermediate state of hydro turbine governor for the third area.

I. INTRODUCTION

Automatic Generation Control (AGC) is a very important control method for maintaining the active power balance within the desired limits in the multi-area power system [1]. The main objectives of AGC control are to maintain the frequency deviations at nominal value, keep the tie-line power changes between areas at a scheduled value, and ensure that the frequency variations are returned to zero [2], [3]. The variation of the daily load and integration of the newly distributed resources, i.e., wind farms and photovoltaic (PV), into the main grid, makes this control even more complex and challenging.

Various control strategies have been developed over the years to solve AGC problems. For example, control strategies such as classical linear control methods problems [4], [5], A fractional $PI^{\lambda}D$ control [6], Adaptive neuro-fuzzy interference system (ANFIS) [7], [8], Robust control methods such as Active disturbance rejection control (ADRC) [9], Variable structure control [10], and H-infinity robust control [11]. For a three-area hydro-thermal power system integrated with distributed energy resources, a Fractional order brain emotional learning-based intelligent controller (FOBELBIC) was proposed to suppress frequency and tie-line deviations [12]. Hybrid type-2 fuzzy logic controllers with fractional order proportional integral derivative (FOPID) have recently been developed to enhance the frequency and tie-line deviations of two control areas under different perturbations [13]. Most of these control methods are designed in the continuous time domain and may be implemented in the discretized time domain. In other words, the measurements of tie-line power and frequency are implemented and delivered as discrete signals to the system control center via communication channels, even though the system is developed based on continuous time modeling [14]; this, however, shows that the AGC controller operates in the discrete-time domain, but the power system operates in the continuous time domain [15]. As a result, the closed-loop performance is poor, which degrades the power system stability. Therefore, a flexible and robust discrete-mode AGC scheme is required, capable of keeping the closed-loop stable and considering the sampling period characteristics of both the AGC controller and the interconnected power system during the design phase [14].

AGC based on modern optimal control theory has been investigated in the literature as one of the control strategies to provide robustness against load disturbances, model uncertainties, and physical constraints. The first optimal AGC control was introduced for two-area interconnected power systems [16], [17]. Reference [18] used hybrid bacteria foraging oriented particle swarm optimization with linear quadratic regulator (LQR) design for interconnected power systems with hydro turbines to test the robustness of the designed controller against step load disturbances, nonlinearities, and parametric variations. The authors in the literature have applied the optimal control theory to control the active power balance of two microgrids interconnected systems with two AC tie-lines [3]. It was proved that optimal AGC control based On LQR can achieve good performance in terms of large stability margins, robustness, and reliability in terms

of nonlinearities in multi-area interconnected power systems [3], [19].

Despite the advantages of optimal AGC-based LQR mentioned above, its performance depends on selecting the state cost weighing matrix (Q) and control cost weighting matrix (R) to obtain the best control efforts and closed-loop performance [18], [20]. State and control signals are penalized when the R and Q value increases. Choosing a large number for the R matrix shows that the designers intended to keep the system stable using less energy (cheap control technique). However, choosing a small number for R implies that the designers are not adjusting the regulator output (cheap control strategy). A more significant Q value means settling the system with the most minor state variation possible, whereas a smaller Q value implies less concern about state deviations.

Several ways for determining state and control weighting matrices have been presented to solve these challenges. The Q and R identity matrices of appropriate dimensions were employed in earlier LQR research. Because of this decision, LQR's control efforts were limited; thus, LQR provided limited action to obtain the best AGC performance [21], [22]. The weighting matrices were selected based on the participation factor analysis, in which states with the most significant participation in relevant modes were given higher weights [23]. Reference [24] calculated the weighting matrices Q and R for LQR using hybrid bacteria foraging-oriented Particle Swarm Optimization (PSO) for hydro system automatic generation control. In another study, weight matrices were chosen based on the controllability and observability indices, and the power system's state matrix was transformed into a diagonal matrix form using the Eigenvalues and Eigenvectors decomposition approach [25]. Most of these methods require an observer to estimate the closed-loop states. Furthermore, state and control input weighting matrices have been constructed using the Functional minimization method (FMM) [25], [26]. In this approach, optimal LQR AGC is designed based on minimizing the cost function for two-area interconnected power systems. The weighting matrices Q and R were defined for the dynamic system under the study by considering the excursion of area control errors, the excursion of the integral of area control errors, and the excursion of the control vector about the steady state. Despite FMM being constructed in the time domain, it provides more realistic responses in a real-time environment for two-area control with communication delays [26]. It is systematic and easy to construct. In addition, because it uses a few numbers of the state variables to construct weighting matrices, it eliminates the need for an observer to estimate the power system states. Therefore, this paper aims to develop a discrete centralized optimal quadratic automatic generation control (COQAGC) for discrete interconnected power systems using optimal control theory, sampling period, and discrete functional minimization method (FMM).

The problem of COQAGC for a discrete two-area interconnected power system based on discrete functional cost minimization is developed in this paper. Moreover, it is compared with existing controllers from the literature.

The main contributions of this paper are as follows:

1. The cost functional minimization is systematically used to select weighing matrices in discrete forms for two control areas, each with identical non-reheat thermal turbines as well as **multi-area multi-source power system**
2. The discrete cost function requirements are defined in terms of area control errors, integral area control errors, and control energy expenditure so that the function of the criterion can be minimized.
3. Discrete centralized optimal quadratic automatic generation control (COQAGC) is designed based on optimal control theory framework and discrete, functional minimization approach for discrete two-area interconnected power systems with load disturbances.
4. The performance of the discrete COQAGC on power system dynamics has been studied with step load perturbations (*SLPs*) and area control errors by considering two identical control areas.

The paper is organized as follows: Section II presents the model of two control areas and the design of the COQAGC controller. Section III describes the developed functional minimization approach in a general framework for N control areas. The results and discussion are described in Section IV, and Section V concludes the paper.

II. PROPOSED DISCRETE CENTRALIZED MODEL OF AGC

Two identical control areas with non-reheat thermal turbines in each area are considered for the study. The proposed discrete centralized optimal closed-loop system of two area interconnected power system is shown in Fig 1. For zero steady-state error, the derivatives of Area Control Areas (*ACEs*) are augmented in the model of two area interconnected power systems. The Integral Area Control Areas (*IACEs*) act as local controllers.

A. DYNAMICS OF TWO-AREA POWER SYSTEM

The state-space model of an interconnected power system can be described [27], [28]:

$$\begin{aligned} \dot{x}(t) &= Ax(t) + Bu(t) + \Gamma w(t) \\ y &= Cx(t) + Du(t) \end{aligned} \tag{1}$$

where $x(t) \in \mathbb{R}^{n\times 1}$ is the state vector, $u(t) \in \mathbb{R}^{2\times 1}$ is the control input vector, and $w(t) \in \mathbb{R}^{2\times 1}$is the load disturbances input vector, whereas A, B, Γ, and C are the respective matrices with appropriate dimensions. The first Ordinary Differential Equations (ODEs) for the different state variables shown in Figure 1 can be derived as follows [28], [29]:

$$\dot{x}_1 = 2\pi T_{12}x_2 - 2\pi T_{12}x_5 \tag{2}$$

$$\dot{x}_2 = -\frac{k_{ps1}}{T_{p1}}x_1 - \frac{1}{T_{ps1}}x_2 + \frac{k_{ps1}}{T_{ps1}}x_3 - \frac{k_{ps1}}{T_{ps1}}\Delta P_{D1} \tag{3}$$

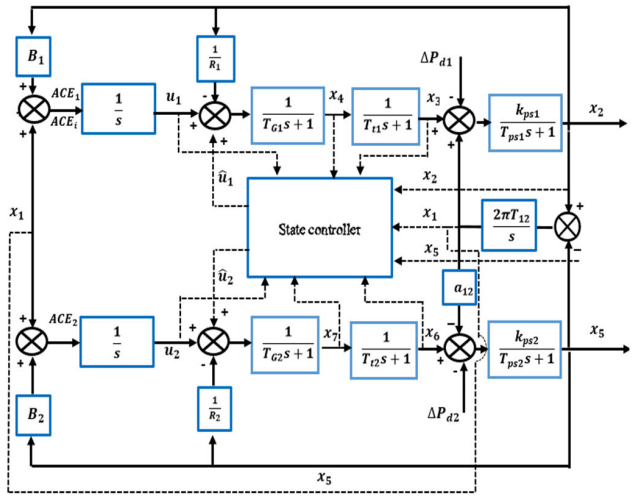

FIGURE 1. Two area control closed-loop system controller.

$$\dot{x}_3 = -\frac{1}{T_{T1}}x_3 + \frac{1}{T_{T1}}x_4 \tag{4}$$

$$\dot{x}_4 = -\frac{1}{T_{G1}R_1}x_2 - \frac{1}{T_{G1}}x_4 + \frac{1}{T_{G1}}u_1 \tag{5}$$

$$\dot{x}_5 = -\frac{a_{12}k_{ps2}}{T_{ps2}}x_1 - \frac{1}{T_{ps2}}x_5 + \frac{k_{ps2}}{T_{ps2}}x_6 - \frac{k_{ps2}}{T_{ps2}}\Delta P_{D2} \tag{6}$$

$$\dot{x}_6 = -\frac{1}{T_{T2}}x_6 + \frac{1}{T_{T2}}x_7 \tag{7}$$

$$\dot{x}_7 = -\frac{1}{T_{G2}R_2}x_5 - \frac{1}{T_{G2}}x_7 + \frac{1}{T_{G2}}u_2 \tag{8}$$

$$\dot{x}_8 = x_1 + \beta_1 x_2 \tag{9}$$

$$\dot{x}_9 = -x_1 + \beta_2 x_5 \tag{10}$$

where,

- x_1: Tie-line deviation between areas 1 and 2
- x_2 and x_5: the deviations in frequency (Hz) for areas 1 and 2 respectively.
- x_3 and x_6: the deviations in the power output of the turbine (pu.MW) for the areas 1and 2 respectively.
- x_4 and x_7: the deviations in the governor valve position (pu.MW) for areas 1 and 2 respectively.

References [28], [30] discussed the derivation procedure of the state space equation of interconnected power systems. As a result, the state space matrices $\boldsymbol{A}, B, \Gamma$, and C for the two control areas with identical non-reheat turbines in each area can be derived as (11), shown at the bottom of the next page, where the state variables are chosen as the tie-line deviation in the tie-line flow ($x_1 = \Delta P_{tie12}$), deviations in frequencies ($x_2 = \Delta f_1, x_5 = \Delta f_2$) in area1 and area2 respectively, the deviation in the power output of turbine1 in area1 ($x_3 = \Delta P_{T1}$), and the deviation in the power output of turbine 2 in area 2 ($x_6 = \Delta P_{T2}$), the deviation in the power output of governor1 in area1 ($x_4 = \Delta P_{G1}$), and the deviation in the power output of governor 2 in area 2 ($x_7 = \Delta P_{G2}$) such that the state, control input, and disturbance input vectors are presented as

$$\begin{aligned} \boldsymbol{x}^T &= \left[\Delta \boldsymbol{P}_{tie12}\ \Delta \boldsymbol{f}_1 \Delta\ \boldsymbol{P}_{T1} \Delta \boldsymbol{P}_{G1}\ \Delta \boldsymbol{f}_2 \Delta\ \boldsymbol{P}_{T2} \Delta\ \boldsymbol{P}_{G2}\right]^T \\ \boldsymbol{u}^T &= [\boldsymbol{u}_1\ \boldsymbol{u}_2]^T \\ \boldsymbol{p}^T &= [\Delta \boldsymbol{P}_{d1}\ \Delta \boldsymbol{P}_{d2}]^T \\ \boldsymbol{y}^T &= \left[\boldsymbol{P}_{tie12} \Delta \boldsymbol{f}_1\ \Delta \boldsymbol{f}_2\right]^T \end{aligned} \tag{12}$$

The linear model of the Tie-line power deviation between areas 1 and 2 can be obtained as follows:

$$\Delta \boldsymbol{P}_{tie12}(\boldsymbol{s}) = \frac{2\pi \boldsymbol{T}_{12}}{\boldsymbol{s}}\left[\Delta \boldsymbol{f}_1 - \Delta \boldsymbol{f}_2\right] \tag{13}$$

B. DESIGN OF DISCRETE COQAGC CONTROL

A linear discrete-time state space equation of the block diagram shown in Fig 1 is given by

$$\begin{aligned} x(k+1) &= A_k x(k) + B_k u(k) + \Gamma_k w(k) \\ x(k_0) &= x_0,\ x\left(k_f\right) = x_{k_f}) \end{aligned} \tag{14}$$

where $x(k)$ is *nth* order state vector, $u(k)$ is *rth* order control vector and A_k and B_k are the time-varying matrices of $n \times n$ and $n \times r$ dimensions, $x(k_0)$ and $x(k_f)$ are the initial and final state conditions respectively , $w(k)$ is *mth* order, and $\Gamma_k \in \mathbb{R}^{n\times r}$ are input load changes vector and a load disturbance matrix respectively.

The steady-state optimization problem of an interconnected power system is to find a control law u, which minimizes a cost function, is given.

$$minJ = \frac{1}{2}\sum_{k=k_0}^{\infty} x^T(k) Q_k x(k) + u^T(k) R_k u(k) \tag{15}$$

Subject to the equality constraint discrete state space model in equation (5).

This optimal feedback gain matrix L can be found by solving the steady-state Riccati matrix equation as follows [30], [31]:

$$L = [R_k + B_k^T P_k B_k]^{-1} B_k^T P_k A_k \tag{16}$$

where P_k is the steady-state Riccati Equation Matrix can be defined as

$$P_k = Q_k + A_k^T \left\{P - P\left[B_k^T P B_k + R_k\right]^{-1} B_k^T P\right\} A_k \tag{17}$$

Substituting the optimal feedback control law in the discrete centralized model of the interconnected power system, the optimal closed-loop system with perturbations is given as follows:

$$x(k+1) = \left[A_k - B_k(\left[R_k + B_k^T P B_k\right]^{-1} B_k^T P A_k)\right] x(k) \tag{18}$$

the closed-loop system will be stable if the real parts of the Eigenvalues of the closed-loop matrix $\left[A_k - B_k[R_k + B_k^T P B_k]^{-1} B_k^T P A_k\right]$ are located in the left half plane of the complex plane.

The flowchart of the COQAGC controller algorithm is shown in Fig. 2. The following steps summarize the detailed methodology of the proposed COQAGC algorithm:

Step 1: Develop and obtain mathematically the state space model of multi-area power systems.

Step 2: Input the model parameters and data for power system simulation.

Step 3: Compute the augmented continuous time matrices.

Step 4: Obtain the discrete-time and augmented matrices obtained in step 3 using Euler's discretization criteria.

Step 5: Initialize the steady Recatti matrix, select the iteration length (M) and select weighting matrices.

Step 6: Calculate the discrete optimal feedback gain matrix and the discrete optimal control law.

Step 7: Initialize the state variables and solve the closed-loop closed loop iteratively using the control law derived in step 6.

*Step 8:*Using MATLAB, simulate the multi-area interconnected power system with COQAGC.

Step 9: Calculate the dynamic response to step load perturbations (SLPs).

Step 10: Repeat step 9 to evaluate the dynamic responses for robustness (parameters uncertainties) and GRC.

III. FUNCTIONAL MINIMIZATION METHOD

In this section, the functional minimization approach will be considered for developing the state and control-weighting matrices (Q_k and R_k). It is a systematic approach consisting of three main steps, namely,

1. The definition of the cost function in terms of the design requirements: Area Control Errors (*ACE*), integral of *ACEs*, and the summation of the individual control efforts [27].
2. Apply the concept of the partial derivatives with respect to each state and each control effort and
3. Combine all first partial derivatives of all states to form the state weighting matrix, and in a similar way, we combine all the partial derivatives of the control efforts to construct the input weighting matrix.

In this approach, the design requirements are transformed to the cost function so that *ACEs*, the integral of *ACEs*, and the control vector u(k) from the steady state are minimized. The steady-state values of *ACEs* are to be zero, while the steady-state values of the integral of *IACEs* and the control vector u are to be constant.

$$
\boldsymbol{A} = \begin{vmatrix}
0 & 2\pi T_{12} & 0 & 0 & -2\pi T_{12} & 0 & 0 & 0 & 0 \\
-\frac{k_{ps1}}{T_{p1}} & -\frac{1}{T_{ps1}} & \frac{k_{ps1}}{T_{p1}} & 0 & 0 & 0 & 0 & 0 & 0 \\
0 & 0 & -\frac{1}{T_{T1}} & \frac{1}{T_{T1}} & 0 & 0 & 0 & 0 & 0 \\
0 & -\frac{1}{R_1 T_{G1}} & 0 & -\frac{1}{T_{G1}} & 0 & 0 & 0 & 0 & 0 \\
-\frac{a_{12}K_{ps2}}{T_{ps2}} & 0 & 0 & 0 & -\frac{1}{T_{ps2}} & \frac{K_{ps2}}{T_{ps2}} & 0 & 0 & 0 \\
0 & 0 & 0 & 0 & 0 & -\frac{1}{T_{T2}} & \frac{1}{T_{T2}} & 0 & 0 \\
0 & 0 & 0 & 0 & -\frac{1}{R_2 T_{G2}} & 0 & \frac{1}{T_{G2}} & 0 & 0 \\
1 & \beta_1 & 0 & 0 & 0 & 0 & 0 & 0 & 0 \\
-1 & 0 & 0 & 0 & \beta_2 & 0 & 0 & 0 & 0
\end{vmatrix},
$$

$$
\boldsymbol{B} = \begin{bmatrix}
0 & 0 \\ 0 & 0 \\ 0 & 0 \\ 0 & 0 \\ 0 & 0 \\ 1 & 0 \\ \frac{T_{G1}}{0} & 0 \\ 0 & 0 \\ 0 & 0 \\ 0 & \frac{1}{T_{F0}}
\end{bmatrix}, \quad
\Gamma = \begin{bmatrix}
0 & 0 \\ -\frac{K_{ps1}}{T_{ps1}} & 0 \\ 0 & 0 \\ 0 & 0 \\ 0 & -\frac{K_{ps2}}{T_{ps2}} \\ 0 & 0 \\ 0 & 0 \\ 0 & 0 \\ 0 & 0
\end{bmatrix}, \quad
C = \begin{bmatrix}
1 & 0 & 0 & 0 & 0 & 0 & 0 & 0 & 0 \\
0 & 1 & 0 & 0 & 0 & 0 & 0 & 0 & 0 \\
0 & 0 & 0 & 0 & 1 & 0 & 0 & 0 & 0
\end{bmatrix} \tag{11}
$$

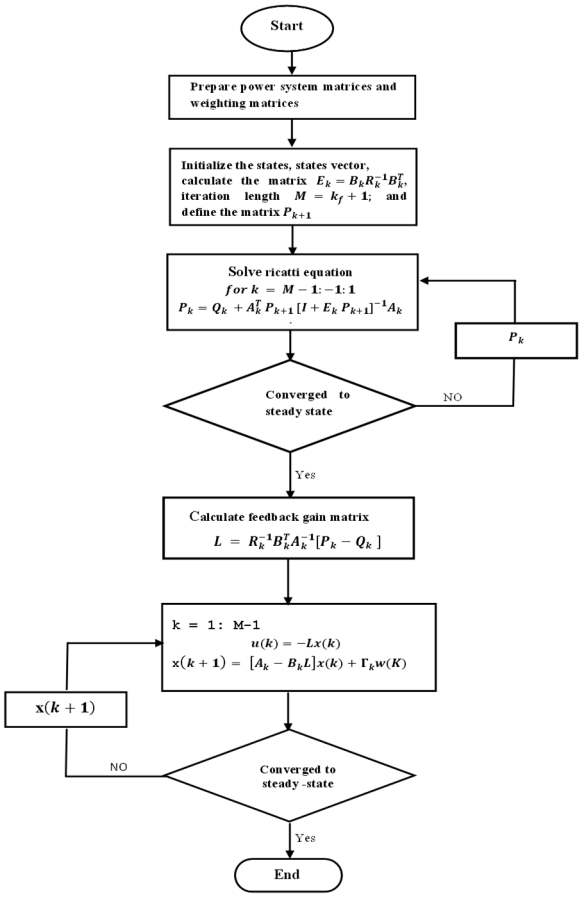

FIGURE 2. Flowchart of COQAGC algorithm.

A. DEVELOPMENT OF STATE MATRIX Q_k

Considering the above design requirements: area control errors, integral of area control errors, and control signals of two control areas, the cost function can be defined as

$$J = \frac{1}{2}\sum_{k=k_0}^{\infty}\left(\left\{(AEC_1)^2 + (AEC_2)^2\right\} + \left\{\left(\sum_{k=k_0}^{\infty} AEC_1\right)^2\right)\right.$$
$$\left.\left(+\left(\sum_{k=k_0}^{\infty} AEC_2\right)^2\right\} + \propto \left\{u_1^2 + u_2^2\right\}\right) \quad (19)$$

where constant $\propto$ is the coefficient that is generally used to limit the control action, in this paper the value of $\propto$ is unity, i.e., $\propto = 1$. Reference [27] defines the area control errors (ACE_1 and ACE_2) and the integral of area control errors ($IACE_1$ and $IACE_2$) of the two control areas, respectively as follows:

$$ACE_1 = \beta_1 \Delta f_1 + \Delta P_{tie12}$$
$$ACE_2 = \beta_2 \Delta f_2 + a_{12}\Delta P_{tie12} \quad (20)$$

and

$$IACE_1 = \sum_{k=k_0}^{\infty}(\beta_1 \Delta f_1 + \Delta P_{tie12})$$
$$IACE_2 = \sum_{k=k_0}^{\infty}(\beta_2 \Delta f_2 + a_{12}\Delta P_{tie2}) \quad (21)$$

Substituting $ACE_1, ACE_2, IACE_1$ and $IACE_2$) to Equation (19) from Equations ((20) and (21)), the cost functional can be given by:

$$J = \frac{1}{2}\sum_{k=k_0}^{\infty}((\beta_1 \Delta f_1 + \Delta P_{tie12})^2$$
$$+ (\beta_2 \Delta f_2 + a_{12}\Delta P_{tie12})^2 + \left\{(IACE_1)^2\right)$$
$$\left(+ (IACE_2)^2\right\} + \propto \left\{u_1^2 + u_2^2\right\}) \quad (22)$$

where β_1 and β_2 are the frequency bias for both areas respectively, ΔP_{tie12} is the tie-line deviation, and $a_{12} = -1$, is the constant coefficient that changes the sign of the tie-line power towards area 2.

Presenting the function of the cost function as a function of the design requirements (*ACEs*, *IACEs* and u), and taking the partial derivatives of the obtained function with respect to state variables, the state weighting matrix Q_k can be derived based on the functional minimization method by combining all states partial derivatives as follows [30]:

$$Q_k = \begin{bmatrix} (1+a_{12}^2) & \beta_1 & 0 & 0 & a_{12}\beta_2 & 0 & 0 & 0 & 0 \\ \beta_1 & \beta_1^2 & 0 & 0 & 0 & 0 & 0 & 0 & 0 \\ 0 & 0 & 0 & 0 & 0 & 0 & 0 & 0 & 0 \\ 0 & 0 & 0 & 0 & 0 & 0 & 0 & 0 & 0 \\ a_{12}\beta_2 & 0 & 0 & 0 & \beta_2^2 & 0 & 0 & 0 & 0 \\ 0 & 0 & 0 & 0 & 0 & 0 & 0 & 0 & 0 \\ 0 & 0 & 0 & 0 & 0 & 0 & 0 & 0 & 0 \\ 0 & 0 & 0 & 0 & 0 & 0 & 0 & 1 & 0 \\ 0 & 0 & 0 & 0 & 0 & 0 & 0 & 0 & 1 \end{bmatrix}$$

B. DEVELOPMENT OF CONTROL WEIGHTING MATRIX R_k

A similar functional minimization method can be applied to control energy expenditure where the first-order partial derivatives with respect to control input signals can be obtained, and control weighing matrix R_k can be constructed as

$$R_k = \begin{bmatrix} 1 & 0 \\ 0 & 1 \end{bmatrix}$$

The power system matrices and state and control weighting matrices (Q_k and R_k)are used further to calculate the o the Optimal Quadratic AGC controller matrix using the Equations (16)-(18).

IV. RESULTS AND DISCUSSIONS

This section tests the developed optimal quadratic AGC controller using MATLAB/Simulink simulation, considering 1%

TABLE 1. The parameters of the two-area thermal power system.

Parameter	Area 1	Area 2	Unit
P_R	2000	2000	MW
T_{ps}	20	20	s
T_t	0.3	0.3	s
K_{ps}	120	120	$Hz/pu\,,MW$
T_{12}	0.0867	0.0867	MW/Hz
T_G	0.08 sec	0.08	s
R_i	2.4	2.4	$Hz/pu\,,MW$
B_i	0.425	0.425	$pu\ MW/Hz$
D_i	0.0833	0.0833	N/m.s
$\Delta\delta$	30°	30°	Degree

step load perturbation (*SLPs*) at $t = 0$ s, 5% concurrent step load perturbation at $t = 5$ s intervals and sensitivity analysis. the power system parameters of the two-area thermal power system given in Table 1 are used to develop the discrete model of two-area power systems considering area control errors (*ACEs*) and MATLAB program is written to obtain the optimal feedback gain matrix L.

A. CALCULATION OF THE DISCRETE MATRICES OF TWO-AREAS POWER SYSTEM

The one-step Euler discretization procedure and sampling time (814 ms) are used to convert the continuous time matrices Aa, Ba and Γa to the discrete-time matrices A_k and B_k given below [32], [33]. The continuous-time and Discrete-time matrices are related with the formulas below in this procedure.

$$\begin{aligned} A_k &= (I + T \times Aa) \\ B_k &= (T \times Ba) \\ \Gamma_k &= (T \times \Gamma a) \end{aligned} \tag{23}$$

where Aa and A_k are augmented continuous and discrete state matrices, respectively, Ba and B_k are augmented continuous and discrete control input matrices, respectively, Γa and Γ_k are augmented continuous and discrete disturbance input matrices, respectively, I is an identity matrix, and T is the sampling period.

B. SIMULATION RESULTS OF CONTROLLED SYSTEM

Referring to Equations (20) to (21), and if $\beta_1 = \beta_2 = 0.425$ and $a_{12} = -1$, *ACEs, IACEs* and for both areas, and the cost function can be obtained. As a result, the function of the cost function can be defined, and the discrete state and control weighting matrices Q_k and R_k are obtained based on the functional minimization procedure next, as shown in the equation at the bottom of the next page.

Then, based on Equation (16), the constant feedback gain matrix value for the closed-loop system at the steady state is found, as shown in the equation at the bottom of the next page.

To assess the feasibility of the proposed controller, the simulation results are compared with other controllers published in the literature, such as Continuous Global Centralized Optimal Quadratic Automatic Generation (GCOQAGC), Teaching Learning-Based Optimization Proportional Integral Double Derivative (TLBO-PIDD) and Fuzzy Gain Scheduling Controller (FGSC) for the same interconnected power system [27], [34], [35].

TABLE 2. Developed controller vs literature control methods in terms peak overshoot (POS) and settling time (STs).

	Case1 (SLPs = 1% pu at t = 0 s)					
	POS (Hz)			STs (s)		
Controller	Δf_1	Δf_2	ΔP_{tie12}	Δf_1	Δf_2	ΔP_{tie12}
Developed COQAGC	0.0276	0.0281	0.0002	4	4	4
FGSC	0.005	0.001	0.0004	0.7	1.2	0.027
TLBO-PIDD	0.13	0. 15	-0.037	6.8	3.9	6.5
GCOQAGCC	-0.13	0.043	--0.017	4	8	8

The dynamic responses of the frequency and tie-line deviations for cases 1 are shown in Figs 3-4. The numerical values of Peak Overshoot (POS) and Settling Times (STs) for frequency deviations (Δf_1 and Δf_2), and tie-line deviations (ΔP_{tie12}) are given in TABLE 2 fort 1% at t = 0 s. The POS values of (frequency deviations (Δf_1 & Δf_2) of FGSC and TLBO-PIDD controllers are (0.0005 & 0.001) and (0.13 & 0.043) respectively and the peak overshoot of tie-line deviations (ΔP_{tie12}) is 0.0004. Meanwhile, the POS values of the developed COQAGC controller of frequency deviations and tie-lie deviations are 0.0276, 0.0281 and 0.0002 respectively. The developed control method can reduce the POS of frequency deviations by up to 79%, 81%, and 50% respectively when compared to TLBO-PIDD controller. On the other hand, the FGSC controller is effective more than the developed COQQAGC control method in terms of POS of frequency deviations (Δf_1 & Δf_2) by up to 82% and 96 % respectively. In terms of peak undershoot values, the developed COQAGC control method can reduce peak undershoot of frequency deviations (Δf_1 & Δf_2) of GCOQAGC and tie-line deviations of TLBO-PIDD by up to 100%, 35%, and 100% respectively when compared to GCOQAGC and TLOBO-PIDD control methods.

In case1 of settling time, the settling time of frequency deviations (Δf_1 & Δf_2), and tie-line deviations (ΔP_{tie12}) using FGSC, TLBO-PIDD, GCOQAGC controllers are (0.7s, 1.2 s & 0.027 s), (6.8 s, 3.9 s & 6.5 s), and (4 s, 8 s & 8 s) respectively. On the other hand, the settling time of the developed control method is 4 s foreach frequency and tie-line deviations. The developed COQAGC control method is able to improve the settling time by up to (83%, 70% & 99%), (41%, −3% & 39), and (0%, 50% & 50%) when compared to FGSC, TLBO_PIDD and GCOQAGC controllers respectively. It can be noted that the developed COQAGC control

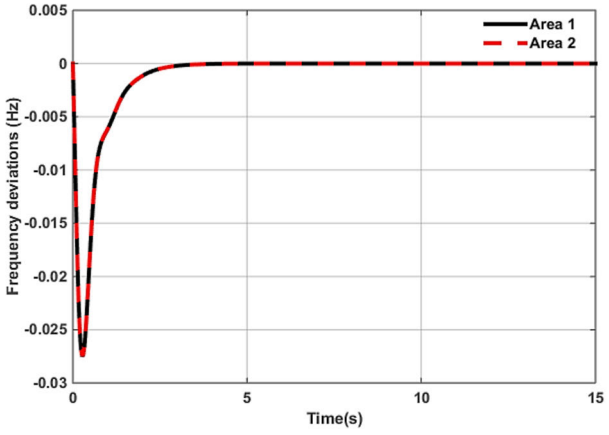

FIGURE 3. Dynamic responses of two control areas for 1% SLP at $t = 0$ s.

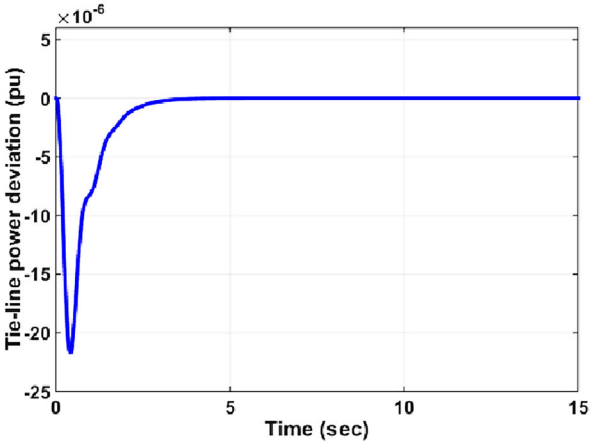

FIGURE 4. Tie-line power deviations response for 1% SLP at $t = 0$ s.

method is slightly less capable i.e., 3% than TLBO-PIDD control method in terms of frequency deviations of control area 2, while the developed COQAGC and GCOQAGC control methods achieved the same settling time in terms of frequency deviation of control area1.

$$A_{ak} = \begin{bmatrix} 1.0000 & 0.0171 & 0 & 0 & -0.0171 & 0 & 0 & 0 & 0 \\ -0.192 & 0.9984 & 0.892 & 0 & 0 & 0 & 0 & 0 & 0 \\ 0 & 0 & 0.8953 & 0.1047 & 0 & 0 & 0 & 0 & 0 \\ 0 & -0.1635 & 0 & 0.6075 & 0 & 0 & 0 & 0 & 0 \\ 0.892 & 0 & 0 & 0 & 0.9984 & 0.1892 & 0 & 0 & 0 \\ 0 & 0 & 0 & 0 & 0 & 0.8953 & 0.1047 & 0 & 0 \\ 0 & 0 & 0 & 0 & -0.1635 & 0 & 0.607525 & 0 & 0 \\ 0.0314 & 0.0133 & 0 & 0 & 0 & 0 & 0 & 1 & 0 \\ -0.0314 & 0 & 0 & 0 & 0.033 & 0 & 0 & 0 & 1 \end{bmatrix}$$

$$B_{ak} = \begin{bmatrix} 0 & 0 \\ 0 & 0 \\ 0 & 0 \\ 0.3925 & 0 \\ 0 & 0 \\ 0 & 0 \\ 0 & 0.3925 \\ 0 & 0 \\ 0 & 0 \end{bmatrix}, \quad \Gamma a = \begin{bmatrix} 0 & 0 \\ -6.024 & 0 \\ 0 & 0 \\ 0 & 0 \\ 0 & -6.024 \\ 0 & 0 \\ 0 & 0 \\ 0 & 0 \\ 0 & 0 \end{bmatrix}$$

$$Q_k = \begin{bmatrix} 2 & 0.425 & 0 & 0 & -0.425 & 0 & 0 & 0 & 0 \\ 0.425 & 0.18063 & 0 & 0 & 0 & 0 & 0 & 0 & 0 \\ 0 & 0 & 0 & 0 & 0 & 0 & 0 & 0 & 0 \\ 0 & 0 & 0 & 0 & 0 & 0 & 0 & 0 & 0 \\ -0.43 & 0 & 0 & 0 & 0.181 & 0 & 0 & 0 & 0 \\ 0 & 0 & 0 & 0 & 0 & 0 & 0 & 0 & 0 \\ 0 & 0 & 0 & 0 & 0 & 0 & 0 & 0 & 0 \\ 0 & 0 & 0 & 0 & 0 & 0 & 0 & 1 & 0 \\ 0 & 0 & 0 & 0 & 0 & 0 & 0 & 0 & 1 \end{bmatrix}, \quad R_k = \begin{bmatrix} 1 & 0 \\ 0 & 1 \end{bmatrix}$$

$$L = \begin{bmatrix} 9.3508 & 9.8614 & 7.9663 & 1.3717 & -1.4092 & -0.6593 & -0.0174 & 17.0789 & 0.2613 \\ -9.3508 & -1.4092 & -0.6593 & -0.0771 & 9.8614 & 7.9663 & 1.3717 & 0.2613 & 17.0789 \end{bmatrix}$$

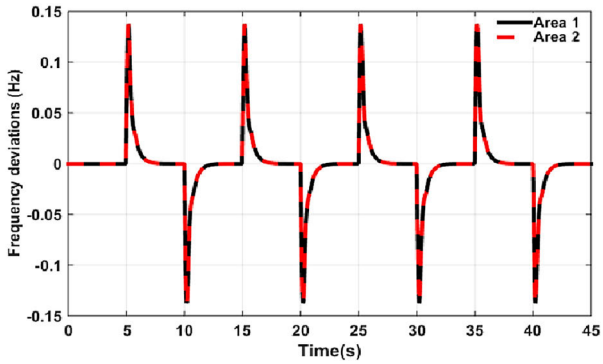

FIGURE 5. Frequency deviations response of COQAGC for two area power systems when SLP of 5% is applied at $t = 5$ s in intervals.

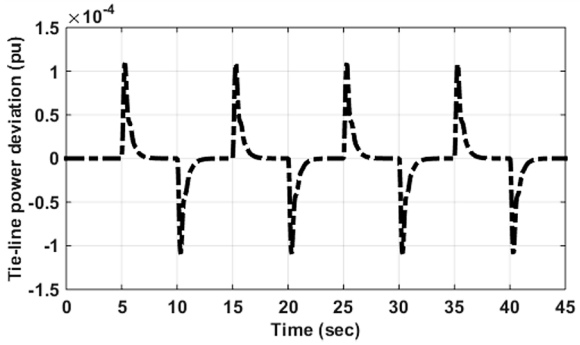

FIGURE 6. Tie-line deviations response between two control areas when SLP of 5% is applied at $t = 5$ s intervals.

It can be observed concluded that COQAGC is the best controller in terms of POS and STs values when compared to TLBO-PIDD and GCOQAGC, while FGSC is best among all controllers in terms of POS and STs values for case1 relating to frequency deviations (Δf_1 and Δf_2).

In case 2, the performance of the proposed controller is studied when concurrent *SLPs* is applied at $t = 5$ *s* intervals. Figs 5 and 6 show the plots of the frequency deviations (Δf_1 *and* Δf_2*)*, and tie-line deviations (ΔP_{tie12}*)*. The numerical values of *POS, STs and* Disturbance Rejection Response Time *(DRRT)* relating to a two non-reheat power system for COQAGC controller are also presented in Table 3, Case 2.

In Table 3, the peak overshoot values of ($\Delta f_1$and Δf_2), and tie-line deviations (ΔP_{tie12}) using GCOQAGC controller are 0.22, 0.03 and -0.003. The proposed control method is able to reduce the POS frequency deviations by up to 87% and 1% respectively. Meanwhile, the settling time values of ($\Delta f_1$and Δf_2), and tie-line deviations (ΔP_{tie12}) using GCOQAGC controller are 5 s each. The DRRT values of the of ($\Delta f_1$and Δf_2), and tie-line deviations (ΔP_{tie12}) using the proposed COQAG-Care 3 s, 3 s, and 2.5 s respectively. The proposed controller able to achieve better disturbance rejection response time (DRRT) for frequency deviations and tie-line deviation by up to 40% and 50%. As result, the COQAGC controller is best in terms of lowest STs, POS and DRRT compared to the GCOQAGC controller. Hence, it can be concluded

TABLE 3. Developed controller vs GCOQAGCC from literature in terms peak overshoot (POS) and settling time (STs).

	Case 2 (SLPs=5% pu at t= 5 s intervals)					
	POS			*DRRT*		
Controller	Δf_1	Δf_2	ΔP_{tie12}	Δf_1	Δf_2	ΔP_{tie12}
Developed COQAGC	*0.028*	*0.028*	*0.008*	*3*	*3*	*2.5*
GCOQAGCC	*0.22*	*0.03*	*-0.003*	*5*	*5*	*5*

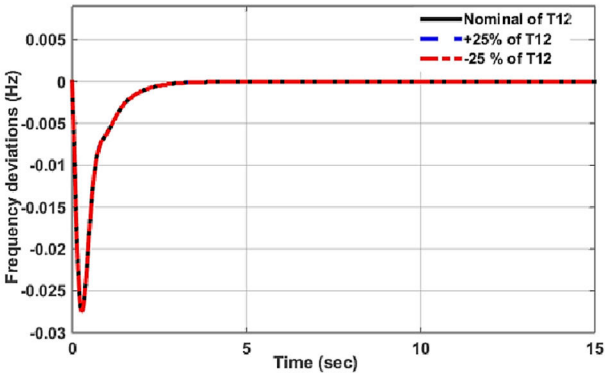

FIGURE 7. Sensitivity analysis response of frequency deviations for variations in tie-line synchronization coefficient.

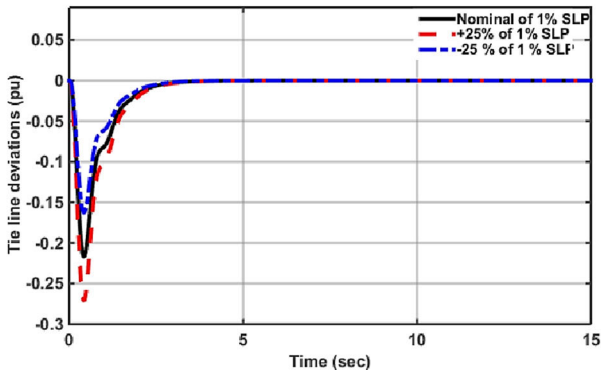

FIGURE 8. Sensitivity analysis response of tie-line for variations in operating load condition.

that the discrete-time COQAGC controller is more capable of providing the lowest POS and STs and is robust against disturbance rejection for the frequency deviations ($\Delta f_1$and Δf_2), and tie-line deviations (ΔP_{tie12}) .

C. SENSITIVITY ANALYSIS

Sensitivity analysis is carried out to test the robustness of the proposed controller at nominal values across variations in operating load conditions and tie-line synchronization coefficient (T_{12}). The *SLPs* and T_{12} are varied from their nominal values by $\pm 25\%$ of their nominal value.

The dynamic responses of the frequency deviations (Δf_1) and tie-line deviations (ΔP_{tie12}) for sensitivity analysis are

TABLE 4. Developed controller vs FGSC controller [35] for sensitivity analysis in terms of peak OS.

	Δf_1			ΔP_{tie12}		
Controller	**Nominal**	**+25%**	**-25%**	**Nominal**	**+25%**	**-25%**
Developed COQAGC	-0.03	-0.03	-0.03	-0.22	0.27	-0.16
FGSC [35]	-0.034	-0.04	-0.05	-0.003	-	0.003

shown in Figs 7-8. The performance of the developed controller is compared to Fuzzy gain Scheduling controller from the literature [33]. This comparison will be done in terms of peak overshoot The numerical values of POS for frequency deviations (Δf_1), and tie-line deviations (ΔP_{tie12}) are given in TABLE 4. It can be observed that both controllers are competitive to each other. In Table 4, the peak undershoots numerical values of the frequency deviation (Δf_1) of the nominal, +25% and −25% of T_{12} using FGSC controller are −0.034. −0.04, −0.05 respectively. Meanwhile, peak undershoot of the nominal, +25% and −25% of T_{12} using the proposed control method are all −0.03. The proposed control method is able to reduce the peak undershoot of frequency deviation (Δf_1) of the nominal, +25% and −25% by 12%,25% and 40% respectively. On the other hand, FGSC is able to reduce peak undershoot (PUS) of tie-line deviation of the nominal value by 99%. As result, COQAGC is the best controller in terms of PUS for variations in tie-line synchronization coefficient, while the FGSC controller is the best in terms of the variations in operating loading conditions. The simulation results in Figs 6 and 7 revealed that COQAGC is robust against the parameter variations.

V. EXTENSION TO MULTI-AREA MULTI SOURCE POWER SYSTEM

To demonstrate the ability of the proposed discrete COQAGC controller, the study is further extended to a multi-area multi-source interconnected power system with renewables as depicted in Figure 9 [30]. Area 1 comprises non-reheat thermal and hydro plants. Area 2 comprises a wind power plant and non-reheat thermal plant. A wind power plant's linear model includes the pitch actuator's transfer function, the lag mechanism's transfer function that matches the model's phase/gain characteristic, and a blade characteristics block [36]. The typical parameters of non-reheat thermals plants are taken from TABLE 1, while wind turbine parameters are adopted from work conducted by Arya & Kumar [37], and Sahu, Griot & Panda [34] and where $T_{p1} = 6$; $T_{p2} = 0.04$, $k_{p2} = 1.25$, $k_{p3} = 1.4$, $T_{g2} = 0.08$, $k_{bc} = 08$, $\mathbb{R}_{\mathrm{w}} = 2.4$ and $\beta_{\mathrm{w}} = 0.425$. On the other hand, the hydro plant parameters are adopted from the work conducted by Parmar, Majhi, & Kothar [38], where $T_w = 1\ s$, $T_{RH} = 0.3\ s$, $T_{RH} = 28.75\ s$, $T_R = 0.11\ s$, $k_{r1} = 0.3$, $T_{gh} = 0.2\ s$,, $T_{r1} = 1\ s$. Note, $k_{ps} = k_{ps1} = k_{ps2} = 120$, $\beta_1 = \beta_2 = \beta_{\mathrm{hy}} = \beta_{\mathrm{w}} = 0.425$, $T_{ps} = T_{ps1} = T_{ps2} = 20$, and $R_1 = R_2 = R_w = R_{hy} = 2.4$for both case studies. The system in Figure 9 has 15 states variables where $x_1 = \Delta f_1$, $x_2 = \Delta P_{GN1}$, $x_3 = \Delta P_{v3}$, $x_4 = IACE_1$, $x_5 = \Delta P_{GH}$, $x_6 = \Delta X_H$, $x_7 = \Delta P_{RH,}$, $x_8 = \Delta P_{tie12}$, $x_9 = \Delta f_2$, $x_{10} = \Delta D$, $x_{11} = \Delta H$, $x_{12} = \Delta H_1$, $x_{13} = IACE_2$, $x_{14} = \Delta P_{GN2}$, $x_{15} = \Delta P_{v4}$.

Reference [30] developed the state, control input, and disturbance vectors, the continuous state matrix $\mathrm{A_m}$, the input matrix $\mathrm{B_m}$, and the disturbance matrix Γ_{m} of a linear state-space model for two area multi-source power systems. Based on the functional minimization method (FMM) in section III, the state and control weighting matrices ($\mathrm{Q_m}$ and $\mathrm{R_m}$) were formulated for a multi-area power system model with renewable energy sources [30]. In this case, the cost function developed by Esmail and Krishnamurthy [30] is considered for the comparison.

$$\begin{aligned} \mathrm{J} = \frac{1}{2}\sum_{\mathrm{k=k_0}}^{\infty} &\left[\mathrm{B_1^2 x_1^2} + 2\beta_1 \mathrm{x_1 x_8} + \mathrm{x_8^2}\right] \\ &+ \left[\mathrm{B_2^2 x_9^2} - 2\beta_1 \mathrm{x_9 x_8} + \mathrm{x_8^2}\right] + (\mathrm{x_4})^2 \\ &+ (\mathrm{x_{13}})^2 + \alpha[\mathrm{U_{th1}^2} + \mathrm{U_{hy}^2} + \mathrm{U_w^2} + \mathrm{U_{th2}^2}] \end{aligned} \tag{24}$$

where α is the vector of participation factors, U_{th1}, U_{hy}, U_w and $\mathrm{U_{th2}}$ are control signals applied to non-reheat thermal 1, hydro, wind turbine, and non-reheat thermal 2 plants, respectively. Similarly, Eq (16) calculates the numerical values of the optimal feedback gains matrix. To study the dynamic response of multi-source power system under COQAGC controller, and step load perturbations (*SLPs*) the following cases are considered.

- Performance comparison with step load perturbations (*SLPs)* 0f 0.01 pu with and without generation rate constraints (GRC) in the model of multi-area multi source power systems.
- Sensitivity analysis to assess robustness of the controllers against ±30% uncertainty in parameter variations.
- Performance comparison with concurrent step load perturbations (*CSLPs*) at 5 s intervals
- Cost function performance comparison with step load perturbation (*SLPs*) of 1% in Area 1 at t= 0 s along with no SLP in Area 2.

A. EFFECT OF GENERATION RATE CONSTRAINT (GRCS)

To study the effect of GRC on dynamic response, 1% *SLPs* are applied at t = 0s [37]. In this test, a GRC for a single non-reheat thermal plant of 10%/min (0.0017pu/s) and a GRC for the hydro plant of 270%/min (+0.045pu/s) for a rising generation, and 360%/min (−0.06pu/s) for a lowering generation for the hydro plant are considered. The system dynamic response is shown in Figs. 10-12. The proposed controller's GRC results, are compared with Optimal full-state feedback control (OFSFC) from the literature [39]. It can be seen from Figs.10-12 that the proposed discrete COQAGC controller gives better dynamic responses, having a relatively smaller peak overshoot and lesser settling time than the Optimal

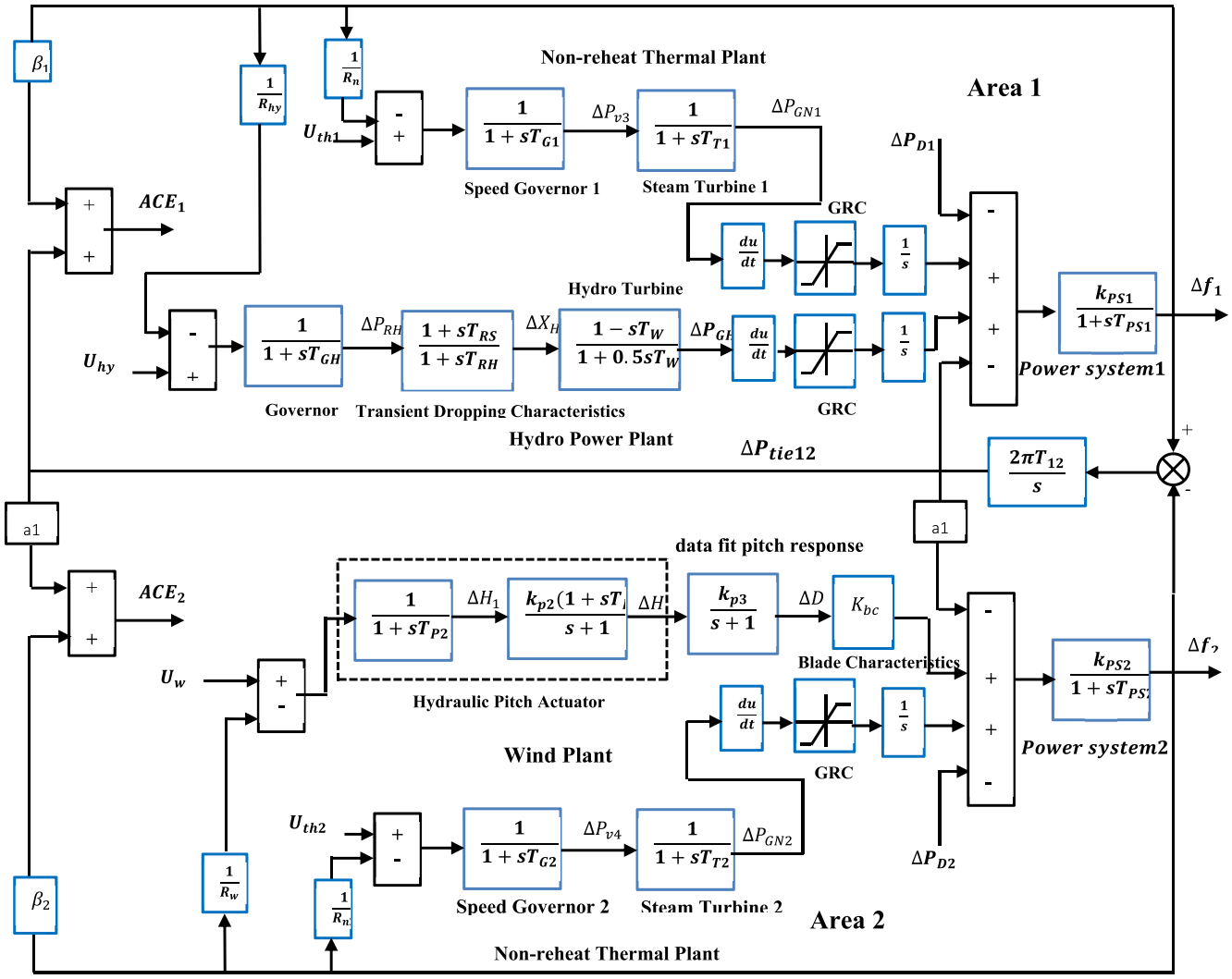

FIGURE 9. Transfer function model of multi-source power system [30].

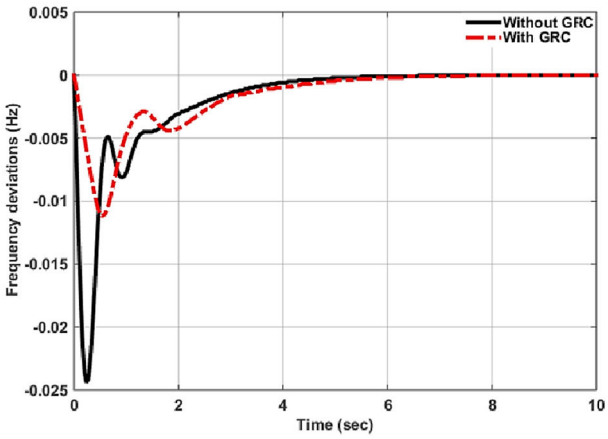

FIGURE 10. Frequency deviation response to 1% SLP in multi-source power system with and without GRC for Area 1.

full state feedback controller. However, OFSFC is somewhat better than COQAGC in terms of peak undershoot.

B. ROBUSTNESS ANALYSIS AGAINST PARAMETER VARIATIONS

In addition to the perturbation of 2% applied in each control area at $t = 0$ s, some parameters are varied to analyse the robustness of the proposed controller. For this purpose, the uncertainty of the -30%, nominal, and $+30\%$ was applied to the significant parameters of the system, such as conducted in the literature [39]. Then, the peak overshoot, peak undershoot, and settling time were evaluated. Figs. 13-15 presents the dynamic response of the proposed controller for frequency and tie-line deviations in terms of nominal parameters and parameter uncertainty of $\pm 30\%$. The results of the proposed controller and LFC-based modified grasshopper optimization algorithm (LFC-MGOA) for nominal and varied parameters considering frequency deviation of area 1 are presented in TABLE 5.

The peak overshoot values of nominal parameters, -30% and $+30\%$ of nominal parameters using LFC-MGOA are 0.0004, 0.00002, and 0.0005 and undershoot values are

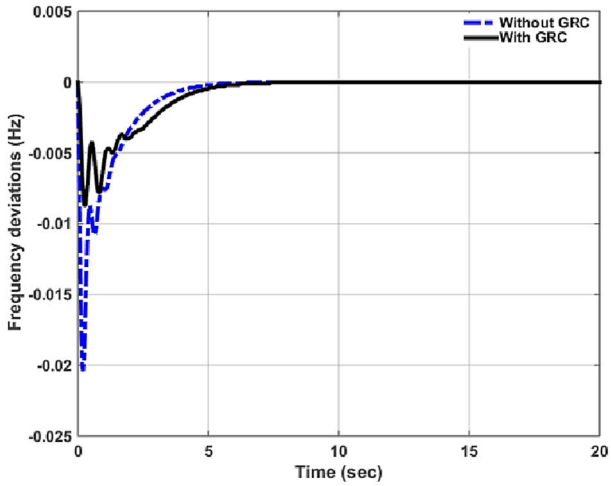

FIGURE 11. Frequency deviation response to 1% SLP in multi-source power system with and without GRC Area 2.

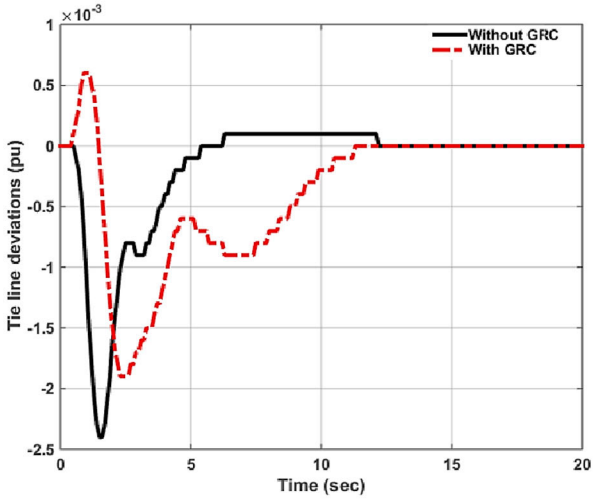

FIGURE 12. Tie-line deviations response to 1% SLP in multi-source power system with and without GRC.

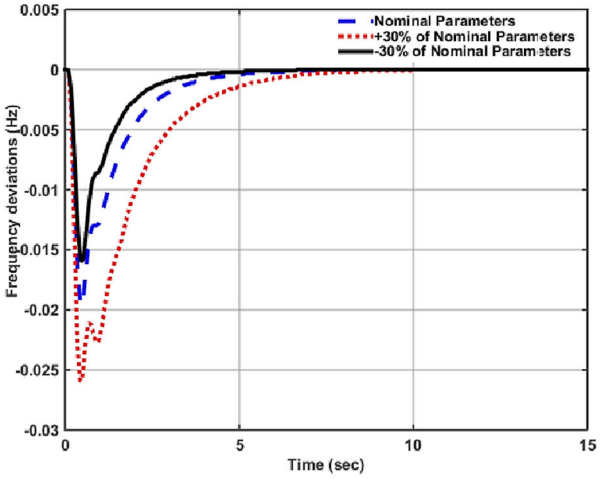

FIGURE 13. Frequency response of area 1 for nominal and uncertainty of ±30%.

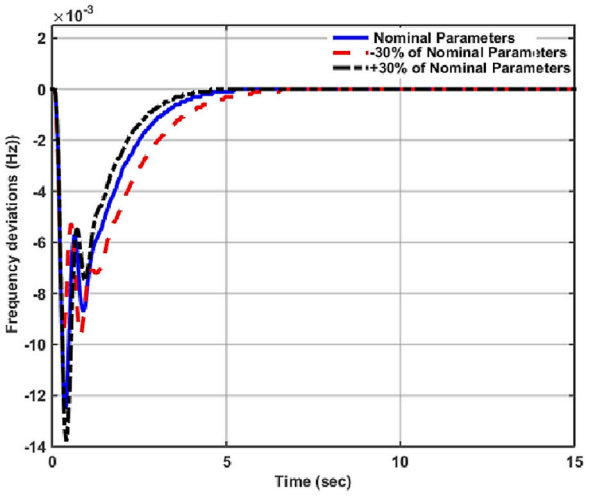

FIGURE 14. Frequency response of area 2 for nominal and uncertainty of ±30%.

−0.022, −0.027, and −0.022. The application of the proposed method is able to reduce the peak overshoot, and peak undershoot by up to (100%, 100%, and 100%), (9% and 41%). LFC-MGOA controller able to reduce the peak undershoot by 15% in comparison to COQAGC. Meanwhile, the settling time of nominal parameters, −30% and +30% of nominal parameters using LFC-MGOA are 10,866 s, 18,01 s, and 22,21 s respectively. The application of COQAGC controller able to reduce settling time by up to 36%, 63%, and 62% respectively. As a result, the proposed controller gives better dynamic performance than LFC-MGOA regarding settling time (STs) and peak overshoot (POS) of all cases. However, if we considered only the instances of nominal and −30%, the peak undershooting value obtained by the proposed controller was also smaller than that of LFC-MGOA by 0.002 Hz and 0.011 Hz, respectively. However, LFC-MGOA gives better undershooting performance for uncertainty of +30%.

C. PERFORMANCE ASSESSMENTS FOR CONCURRENT STEP LOAD PERTURBATIONS

In this section, concurrent step load perturbations with interval of 5 s and amplitude of 0.01 pu are applied in areas 1 and 2. The dynamic response of the frequency deviations and tie-line deviations are presented in Figs 16 and 17 respectively.,

The simulation results for frequency deviations and tie-lie power deviations of both areas are summarized in Tables 6. It is observed that the discrete COQAGC controller achieves almost the same frequency deviation responses of peak overshoots when the concurrent Step Load Perturbations ($SLPs = 0.01$pu) are applied at t = 5 s intervals. The area 2 has 18 % difference of peak overshoot compared to that of area1. The settling time of area 2 is smaller than the settling time of area 1 with zero steady state errors in both cases. The settling time

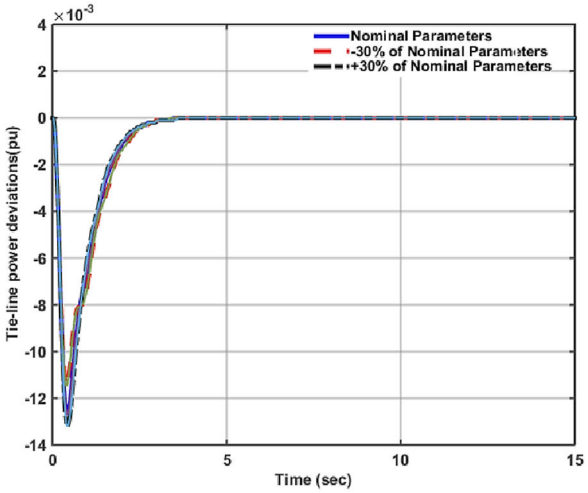

FIGURE 15. Tie-line deviation response between areas 1 and 2 for nominal and uncertainty of ±30.

TABLE 5. Results of developed controller vs MGA from literature in terms peak overshoot (POS), peak undershoot (PUS) and settling time (STs).

	COQAGC (Developed)			LFC-MGOA [39]		
	STs (s)	POS	PUS	STs (s)	POS	PUS
Nominal	7	0	-0.02	10.866	0.0004	-0.022
-30%	7	0	-0.016	18,01	0.0002	-0.027
+30%	8.5	0	-0.026	22.21	0.0005	-0.022

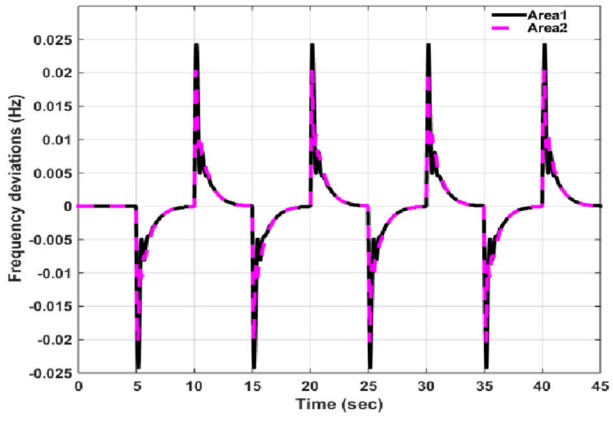

FIGURE 16. Frequency deviation results of two areas 1 and 2 with simultaneous SLPs.

and peak overshoot are same for the tie-line power deviations. The tie line deviation has lesser disturbance rejection time response when compared to disturbance rejection time response of the frequency deviations.

D. APPLYING SLP OF 1% IN AREA 1 AT T = 0 S ALONG WITH NO SLP IN AREA 2

Step load perturbations (SLPs) of 1% is applied in area 1 at t = 0 s with no SLP in area 2 to evaluate the performance

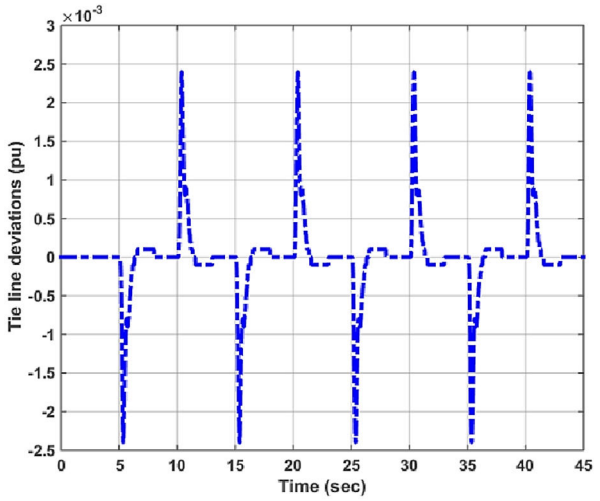

FIGURE 17. Tie-line power deviation result in both areas with simultaneous SLPs.

TABLE 6. Performance of COQAGC in terms of POS, TS, DRRT) and Steady state error ($e_{ss}(\infty)$) with concurrent SLPs.

Frequency Deviations					
Controller	Area	ST (s)	POS	DRRT (s)	$e_{ss}(\infty)$
DOQAGC (developed)	1	4.95	-0.0244	4.85	0
	2	4.875	-0.0201	4.925	0
Difference %	-	2%	18%	2%	```````
Tie-line power deviations (pu)					
DOQAGC	1 and 2	3.05	-0.0024	3.05	0

TABLE 7. Comparative performance of cost function and settling time for multi-area multi-source power systems.

Controller	TS (2% band) s			Cost function J
	$\Delta f1$	$\Delta f2$	$\Delta Ptie12$	
TLBO-PIDD	16.14	16.79	12.77	ITAE = 0.4543
DOQAGC	5	5.4	3.5	FMM = 0.00067
Difference %	69 %	68 %	73 %	99 %

of the cost function. Two types of cost functions are compared, namely, based on Integral Multiplied Time Absolute Error (ITAE) and functional minimization method. The cost function values for COQAGC and TLBO-PIDD controller from the literature are presented in Table 7. From Table 7 it can be observed that minimum FMM values is obtained with the developed COQAGC controller (FMM = 0.00067) when compared to TLBO-PIDD (ITAE = 0.4543). Further, it can be clearly seen from Table 7 that the frequencies and tie-line deviations are improved with COQAGC compared to TLBO-PIDD. It can be concluded that is better than TLBO-PIDD by up to 69%, 68% and 73% in frequencies and tie-line deviations respectively as well as by up to 99% in cost function performance.

VI. CONCLUSION

The optimal control theory and Lagrangian traditional multipliers method have been utilized to develop discrete time centralized optimal quadratic automatic generation control (COQAGC) for a discrete-time two-area power system and multi-area multi-source power systems. The model of a two-area power system with two identical non-reheat turbines has been considered. For zero steady-state errors, the derivatives of area control errors have been added to the state vector of the model of the considered interconnected power systems.

The functional minimization method is utilized to develop discrete COQAGC by considering area control errors, integral of area control errors, and control energy expenditure. In return, COQAGC minimizes the cost function, and the power system closed loop of the interconnected power system. The functional minimization method is a systematic approach, optimal, and easy to derive for constructing the state and controlling weighting matrices.

The simulation results revealed that the discrete centralized optimal quadratic AGC controller based on functional cost minimization is robust against disturbance and sensitivity analysis compared with controllers from the literature

The developed control method is based on well-known quadratic optimal control theory and its application can be extended to solve AGC problems in more complex interconnected power systems.

ACKNOWLEDGMENT

The authors gratefully acknowledge the authorities of the Cape Peninsula University of Technology, South Africa, for the facilities offered to carry out this work.

REFERENCES

[1] R. Shankar, S. R. Pradhan, K. Chatterjee, and R. Mandal, "A comprehensive state of the art literature survey on LFC mechanism for power system," *Renew. Sustain. Energy Rev.*, vol. 76, pp. 1185–1207, Sep. 2017.

[2] M. T. Alrifai, M. F. Hassan, and M. Zribi, "Decentralized load frequency controller for a multi-area interconnected power system," *Int. J. Electr. Power Energy Syst.*, vol. 33, no. 2, pp. 198–209, Feb. 2011.

[3] D. H. Tungadio, R. C. Bansal, and M. W. Siti, "Optimal control of active power of two micro-grids interconnected with two AC tie-lines," *Electr. Power Compon. Syst.*, vol. 45, no. 19, pp. 2188–2199, Nov. 2017.

[4] M. Esmail, R. Tzoneva, and S. Krishnamurthy, "Review of automatic generation control in deregulated environment," *IFAC-PapersOnLine*, vol. 50, no. 2, pp. 88–93, Dec. 2017.

[5] W. Tan and Z. Xu, "Robust analysis and design of load frequency controller for power systems," *Electr. Power Syst. Res.*, vol. 79, no. 5, pp. 846–853, May 2009.

[6] A. Delassi, S. Arif, and L. Mokrani, "Load frequency control problem in interconnected power systems using robust fractional PI$^{\lambda}$D controller," *Ain Shams Eng. J.*, vol. 9, no. 1, pp. 77–88, Mar. 2018.

[7] S. R. Khuntia and S. Panda, "Simulation study for automatic generation control of a multi-area power system by ANFIS approach," *Appl. Soft Comput.*, vol. 12, no. 1, pp. 333–341, Jan. 2012.

[8] S. Prakash and S. K. Sinha, "Simulation based neuro-fuzzy hybrid intelligent PI control approach in four-area load frequency control of interconnected power system," *Appl. Soft Comput.*, vol. 23, pp. 152–164, Oct. 2014.

[9] L. Dong, Y. Zhang, and Z. Gao, "A robust decentralized load frequency controller for interconnected power systems," *ISA Trans.*, vol. 51, no. 3, pp. 410–419, May 2012.

[10] W. Chan, S. Mem, and Y. Hsu, "Automatic generation control of interconnected power systems using variable-structure controllers," *IEE Proc. D, Control Theory Appl.*, vol. 138, no. 6, pp. 579–585, 1981.

[11] Z.-Q. Wang and M. Sznaier, "Robust control design for load frequency control using μ synthesis," in *Proc. Conf. Rec. Southcon*, Orlando, FL, USA, Mar. 1994, pp. 186–190.

[12] A. D. Falehi, "Optimal fractional order BELBIC to ameliorate small signal stability of interconnected hybrid power system," *Environ. Prog. Sustain. Energy*, vol. 38, no. 5, pp. 1–18, Sep. 2019.

[13] A. D. Falehi, "Robust and intelligent type-2 fuzzy fractional-order controller-based automatic generation control to enhance the damping performance of multi-machine power systems," *IETE J. Res.*, vol. 68, no. 4, pp. 2548–2559, Jul. 2022.

[14] X. Shang-Guan, Y. He, C. Zhang, L. Jiang, and J. W. Spencer, "Sampled-data based discrete and fast load frequency control for power systems with wind power," *Appl. Energy*, vol. 259, Jan. 2020, Art. no. 114202.

[15] H. Bevrani, *Robust Power System Frequency Control*, 2nd ed. Cham, Switzerland: Springer, 2014.

[16] K. Vrdoljak, N. Perić, and I. Petrović, "Sliding mode based load-frequency control in power systems," *Electr. Power Syst. Res.*, vol. 80, no. 5, pp. 514–527, May 2010.

[17] O. Elgerd and C. Fosha, "Optimum megawatt-frequency control of multi-area electric energy systems," *IEEE Trans. Power App. Syst.*, vol. PAS-89, no. 4, pp. 556–563, Apr. 1970.

[18] C. Fosha and O. Elgerd, "The megawatt-frequency control problem: A new approach via optimal control theory," *IEEE Trans. Power App. Syst.*, vol. PAS-89, no. 4, pp. 563–577, Apr. 1970.

[19] A. Panwar, V. Agarwal, G. Sharma, and S. Sharma, "Design of a novel AGC action for a linked hydro governing system," *Electr. Power Compon. Syst.*, vol. 49, no. 15, pp. 1201–1211, Sep. 2021.

[20] E. Vlahakis, L. Dritsas, and G. Halikias, "Distributed LQR design for a class of large-scale multi-area power systems," *Energies*, vol. 12, no. 14, p. 2664, Jul. 2019.

[21] Y. Arya, N. Kumar, and S. K. Gupta, "Optimal automatic generation control of two-area power systems with energy storage units under deregulated environment," *J. Renew. Sustain. Energy*, vol. 9, no. 6, Nov. 2017, Art. no. 064105.

[22] G. Sharma, I. Nasiruddin, K. R. Niazi, and R. C. Bansal, "Robust automatic generation control regulators for a two-area power system interconnected via AC/DC tie-lines considering new structures of matrix *Q*," *IET Gener., Transmiss. Distrib.*, vol. 10, no. 14, pp. 3570–3579, Nov. 2016.

[23] G. Sharma, "Optimal AGC design for diverse sources of power generations in each area using output vector feedback control technique," *Int. J. Eng. Res. Afr.*, vol. 45, pp. 99–114, Nov. 2019.

[24] A. Prakash, P. Singh, K. Kumar, and S. K. Parida, "Design of a reduced-order WADC for wind turbine system-integrated power system," *IEEE Trans. Ind. Appl.*, vol. 58, no. 3, pp. 3250–3260, May 2022.

[25] Y. Arya, "A new optimized fuzzy FOPI-FOPD controller for automatic generation control of electric power systems," *J. Franklin Inst.*, vol. 356, no. 11, pp. 5611–5629, Jul. 2019.

[26] N. H. Ibraheem and P. Kumar, "Optimal automatic generation control of interconnected power system considering new structures of matrix *Q*," *Electr. Power Compon. Syst.*, vol. 41, no. 2, pp. 136–156, Jan. 2013.

[27] N. Pathak, I. Nasiruddin, and T. S. Bhatti, "A more realistic model of centralized automatic generation control in real-time environment," *Electr. Power Compon. Syst.*, vol. 43, no. 19, pp. 2205–2213, Nov. 2015.

[28] E. Rakhshani, D. Remon, A. M. Cantarellas, and P. Rodriguez, "Analysis of derivative control based virtual inertia in multi-area high-voltage direct current interconnected power systems," *IET Gener., Transmiss. Distrib.*, vol. 10, no. 6, pp. 1458–1469, Apr. 2016.

[29] M. Deepak and R. J. Abraham, "Load following in a deregulated power system with thyristor controlled series compensator," *Int. J. Electr. Power Energy Syst.*, vol. 65, pp. 136–145, Feb. 2015.

[30] M. Esmail and S. Krishnamurthy, "Discrete optimal quadratic AGC based cost functional minimization for interconnected power systems," *Sci. Rep.*, vol. 13, no. 1, pp. 1–37, Feb. 2023.

[31] D. S. Naidu, *Optimal Control System*. Boca Raton, FL, USA: CRC Press, 2002.

[32] M. Kögel and R. Findeisen, "Discrete-time robust model predictive control for continuous-time nonlinear systems," in *Proc. Amer. Control Conf. (ACC)*, Chicago, IL, USA, Jul. 2015, pp. 924–930.

[33] E. Boukas and F. M. AL-Sunni, *Mechatronic Systems: Analysis, Design and Implementation*. Berlin, Germany: Springer, 2011.
[34] R. K. Sahu, T. S. Gorripotu, and S. Panda, "Automatic generation control of multi-area power systems with diverse energy sources using teaching learning based optimization algorithm," *Eng. Sci. Technol., Int. J.*, vol. 19, no. 1, pp. 113–134, Mar. 2016.
[35] Y. Arya and N. Kumar, "Fuzzy gain scheduling controllers for automatic generation control of two-area interconnected electrical power systems," *Electr. Power Compon. Syst.*, vol. 44, no. 7, pp. 737–751, Apr. 2016.
[36] D. Das, S. K. Aditya, and D. P. Kothari, "Dynamics of diesel and wind turbine generators on an isolated power system," *Int. J. Electr. Power Energy Syst.*, vol. 21, no. 3, pp. 183–189, Mar. 1999.
[37] Y. Arya and N. Kumar, "AGC of a multi-area multi-source hydrothermal power system interconnected via AC/DC parallel links under deregulated environment," *Int. J. Electr. Power Energy Syst.*, vol. 75, pp. 127–138, Feb. 2016.
[38] K. P. S. Parmar, S. Majhi, and D. P. Kothari, "Load frequency control of a realistic power system with multi-source power generation," *Int. J. Electr. Power Energy Syst.*, vol. 42, no. 1, pp. 426–433, Nov. 2012.
[39] S. Gouran-Orimi and A. Ghasemi-Marzbali, "Load frequency control of multi-area multi-source system with nonlinear structures using modified grasshopper optimization algorithm," *Appl. Soft Comput.*, vol. 137, Apr. 2023, Art. no. 110135.

MOHAMMED ESMAIL received the B.Sc. degree (Hons.) in electronics engineering technology from the University of Gezira (UoG), Wad Madani, Sudan, in 2001, the M.Sc. degree in biomedical engineering from the University of Cape Town (UCT), Cape Town, South Africa, in 2013, and the Ph.D. degree in electrical engineering from the Cape Peninsula University of Technology (CPUT), in December 2023.

From 2017 to 2019, he was a part-time Lecturer with the Centre for Substation Automation and Energy Management Systems (CSAEMS), CPUT. Since 2013, he has been a Lecturer with the Department of Mechanical and Mechatronic Engineering, CPUT. His research interests include smart grid optimization and control, integrated distributed energy resource technologies, conventional interconnected power systems, dynamical modeling of complex interconnected power systems, and point-to-point positioning applications.

SENTHIL KRISHNAMURTHY (Member, IEEE) received the B.Eng. and M.Eng. degrees in power systems from Annamalai University, India, in 2006 and 2008, respectively, and the Ph.D. degree in electrical engineering from Cape Peninsula University of Technology (CPUT), Cape Town, South Africa, in 2013.

He has been an Associate Professor with the Department of Electrical, Electronic and Computer Engineering, CPUT. He heads the Cluster of Power Systems and the Deputy Leader of the Centre for Substation Automation and Energy Management Systems (CSAEMS), supported by the National Research Foundation (NRF). He has received several industrial grants, among them the ESKOM TESP EPPEI, SANEDI JET, and NRF Thuthuka. His research interests include power systems, AI-based optimization methods, protective relaying systems, substation automation, renewable energy, energy management systems, and parallel computing. He is a Registered Professional Engineer with the Engineering Council of South Africa (ECSA), a member of the Institute of Engineers in India (IEI), and a Senior Member of the South African Institute of Electrical Engineers (SAIEE).